Pacific Northwest
NATIONAL LABORATORY

PNNL-36585, Rev 0
DVZ-RPT-112, Rev 0

Monitoring of In Situ Remediation Technologies with SIP

December 2024

Hilary Emerson
Jonathan Thomle
Zoe Vincent
Judy Robinson
Josh Torgeson
Klaudio Peshtani
Nikolla Qafoku
Jim Szecsody
Fred Day-Lewis
Lee Slater

U.S. DEPARTMENT OF ENERGY

Prepared for the U.S. Department of Energy
under Contract DE-AC05-76RL01830

DISCLAIMER

PACIFIC NORTHWEST NATIONAL LABORATORY
operated by
BATTELLE
for the
UNITED STATES DEPARTMENT OF ENERGY
under Contract DE-AC05-76RL01830

Printed in the United States of America

Available to DOE and DOE contractors from the
Office of Scientific and Technical Information,
P.O. Box 62, Oak Ridge, TN 37831-0062;
ph: (865) 576-8401
fax: (865) 576-5728
email: reports@adonis.osti.gov

Available to the public from the National Technical Information Service
5301 Shawnee Rd., Alexandria, VA 22312
ph: (800) 553-NTIS (6847)
email: orders@ntis.gov <https://www.ntis.gov/about>
Online ordering: http://www.ntis.gov

PNNL-36585, Rev 0
DVZ-RPT-112, Rev 0

Monitoring of In Situ Remediation Technologies with SIP

FY24 Status Report

December 2024

Hilary Emerson
Jonathan Thomle
Zoe Vincent
Judy Robinson
Josh Torgeson
Klaudio Peshtani
Nikolla Qafoku
Jim Szecsody
Fred Day-Lewis
Lee Slater

Prepared for
the U.S. Department of Energy
under Contract DE-AC05-76RL01830

Pacific Northwest National Laboratory
Richland, Washington 99354

Summary

Deconvoluting spectral induced polarization (SIP) signals is critical to developing SIP as a robust technology to monitor delivery and subsequent geochemical reactions in the subsurface. Therefore, the primary objective of this project is to elucidate the sensitivity of SIP to specific geochemical reactions occurring during subsurface remediation based on their impact on polarization of minerals and their surfaces. This document outlines progress for fiscal year (FY) 2024 toward validating SIP for monitoring specific reactions related to remediation at the laboratory scale. This work aims to advance the technology to field-scale for monitoring of amendment delivery and subsequent reactivity for subsurface remediation. An interdisciplinary critical review team was assembled to review historical SIP data collected under the Deep Vadose Zone program.

Based on feedback from the team, additional experiments were designed and initiated for the calcium citrate phosphate technology for in situ formation of apatite, and additional analysis was conducted with data from sulfur modified iron experiments to consider the potential for scaling monitoring with SIP to the field. Preliminary laboratory scale results showed a significant decrease in SIP response due to apatite formation in 1D column experiments. Synthetic field data was generated on 2 m × 2 m × 2 m blocks placed 1 m and 2.5 m below the ground surface, based on previous laboratory scale experiments. The results showed that changes in SIP response due to delivery of sulfur modified iron could be measurable at specific frequencies in the field.

In addition, the team outlined a proposed framework for future evaluation of SIP for environmental remediation monitoring to be implemented over the next 2-3 years. The framework was laid out based on two broad knowledge gaps in (i) our fundamental understanding of SIP and (ii) moving SIP from laboratory to field scale for monitoring of delivery and reactivity of amendments. For the first knowledge gap, the scope outlined included well-characterized microfluidics experiments to interpret and model SIP responses based on different geochemical reactions and processes. For the second knowledge gap, additional 1D and 2D experiments spanning up to intermediate scale (cm to m) were recommended to consider the impact of subsurface heterogeneity and amendment delivery on SIP response.

Acknowledgments

This document was prepared by the Deep Vadose Zone – Applied Field Research Initiative at Pacific Northwest National Laboratory. Funding was provided by the U.S. Department of Energy (DOE) Richland Operations Office. Pacific Northwest National Laboratory is operated by Battelle Memorial Institute for the DOE under Contract DE-AC05-76RL01830.

The authors acknowledge project manager Rob Mackley of the Deep Vadose Zone – Applied Field Research Initiative for championing this effort and Matt Wilburn for technical editing. The authors also thank the entire critical review team for their thoughtful feedback and ideation, including Fred Day-Lewis, Inci Demirkanli, Timothy C. Johnson, Rob Mackley, Klaudio Peshtani, Nikolla Qafoku, Judy Robinson, Lee Slater, Chris Strickland, Jonathan Thomle, and Chao Zeng.

Acronyms and Abbreviations

BET	Brunauer–Emmett–Teller
Ca-Cit-PO_4	calcium citrate phosphate solution
CEC	cation exchange capacity
E4D	3D geophysical modeling and inversion code
EDL	electrical double layer
ERT	electrical resistivity tomography
FY	fiscal year
Hf	Hanford formation
MDL	minimum detection limit
pXRD	X-ray diffraction of powdered samples
QAQC	quality assurance and quality control
SGW	synthetic groundwater
SIP	spectral induced polarization
SMI	sulfur modified iron
XCT	X-ray computed microtomography
XMCD	X-ray magnetic circular dichroism

Contents

Figures

Tables

1.0 Introduction

There is a need for non-invasive and cost-effective technologies to monitor and understand the delivery and efficacy of field-scale remediation. Spectral induced polarization (SIP) is an emerging geophysical technology that could used for this purpose because it can provide information on where the chemical reactions targeted during remediation are occurring and how they are progressing. SIP is similar to electrical resistivity tomography (ERT), which measures bulk electrical conductivity and has been successfully used at the Hanford Site to characterize the location of remedial injection solutions in the vadose zone and in groundwater. However, while ERT is similarly sensitive to changes in subsurface pore fluid chemistry and the electrical double layer (EDL) or the mineral-fluid interfacial region of the electrically charged soil minerals, these two different effects cannot be separated using ERT. SIP, however, measures complex conductivity (conductivity and phase) across a range of frequencies, providing additional data that has demonstrated sensitivity to both pore fluid chemistry and mineral surface reactions of interest in subsurface remediation (Binley and Slater, 2020; Dias, 2000). SIP has the potential for subsurface monitoring of remediation technology injection, precipitation, and other geochemical reactions that occur at the mineral-surface interface.

Deconvoluting peaks observed in the SIP signal is critical to developing SIP as a robust technology to monitor delivery and subsurface geochemical reactions. A fundamental understanding of the SIP response is paramount for interpreting SIP signals in terms of the complex reactions occurring during remediation of the subsurface. Therefore, the primary goal of this project is to elucidate the sensitivity of SIP to specific geochemical reactions occurring during subsurface remediation. Geochemical changes occur both during and after delivery of an amendment as intended reactions occur and efficacy changes over time. For example, initial delivery of a reductive amendment like sulfur modified iron (SMI) should generate reducing conditions that alter natural minerals present in the subsurface while the SMI also changes over time as oxidation and corrosion occur.

This document presents progress for fiscal year (FY) 2024 toward field-scale SIP monitoring of amendment delivery and reactivity for subsurface remediation.

1.1 Objectives

A critical review team was assembled to develop objectives and action items to advance SIP from an emerging technology primarily used in the laboratory to a technology demonstration for field-scale monitoring. The objectives are to collect and collate data at the laboratory scale to demonstrate that SIP can be used to monitor specific geochemical reactions induced by amendments for subsurface remediation and that the technology can be scaled up to the field effectively. For FY24, objective were (i) review historical data, (ii) identify additional technology development and demonstration activities, (iii) outline a multi-year approach, and (iv) begin implementing this approach, with specific action items to address the remaining questions impeding the use of SIP for field-scale monitoring of subsurface remediation activities.

The major outcomes after the next 2-3 years of work include a library of laboratory-scale experimental data and modeling demonstrating the potential (or lack thereof) for monitoring specific amendments and intermediate-scale experimental data and modeling (with upscaling to field conditions) demonstrating the subsurface conditions where SIP could (or should not) be used for field-scale monitoring.

1.2 FY24 Achievements

Milestone achievements are summarized below. These achievements, in addition to the preliminary experimental and modeling results presented in Section 3.0, helped the development of recommendations for future work outlined in Section 4.0.

- The critical review team consisting of an interdisciplinary group of subject matter experts across geophysics, geochemistry, hydrology, and engineering identified the major knowledge gaps remaining to develop SIP as a field-scale technology for monitoring remediation (Section 4.0). Hybrid meetings were conducted to evaluate SIP data collected previously monitoring the injection of remedial amendments.
- Data review and analysis tools were developed and used to improve the workflow for processing and visualizing SIP data using Python codes, R codes, and MATLAB routines. Staff were trained on SIPy Studio software (https://sgs4d.com/product/sipy-studio/), which can fit theoretical models (e.g., Cole-Cole and Debye decomposition) to the SIP data. These tools were used to critically evaluate data collected previously (FY20-FY22) under the Deep Vadose Zone program. Results were presented during review meetings with subject matter experts to evaluate the results and determine the path forward for future work.

As a direct result of these milestone achievements, additional highlights are summarized below.

- The critical review team identified knowledge gaps in the SIP experiments with calcium citrate phosphate (Ca-Cit-PO_4), which is a method of forming apatite in the subsurface to reduce the mobility of contaminants. The design of the columns and electrodes was improved (summary in Section 2.1 with details in Appendix A, Section A.3), and laboratory data was collected using these new designs. Preliminary results are presented in Section 3.1 with the materials and methods in Appendix A.
- A numerical modeling exercise was conducted using laboratory-scale data collected for SMI mixed with Hanford formation (Hf) sediments to investigate the potential for detection of SMI at 10 wt% at the field scale. These results highlight the potential for SIP for monitoring geochemical reactions at the field scale under specific conditions when there is a frequency-dependent SIP response. Preliminary results are presented in Section 3.2.
- To better understand and evaluate the current state of knowledge of SIP, an extensive literature review was conducted with a focus on our ability to interpret geochemical changes over time. A review paper is nearly complete for submittal to *Critical Reviews in Environmental Science and Technology* (target date for submission: February 2025). A conceptual diagram has been developed that summarizes our literature review (Section 2.1, Figure 1).

The project also had considerable engagement with early-career staff and notable technical output.

- Interns and early career staff were mentored and trained in experimental procedures and data analysis for this project, including:
  - Zoe Vincent (Post Bachelor's, BS environmental science, Northwestern University)
  - Klaudio Peshtani (DOE-EM MSIPP[1] Postdoctoral Associate, PhD environmental science, Rutgers University – Newark)

[1] U.S. Department of Energy Office of Environmental Management Minority Serving Institution Partnership Program.

  - Suraj Pochampally (DOE-EM MSIPP Postdoctoral Associate, PhD mechanical engineering, University of Nevada, Las Vegas)
  - Minbum Kim (Postdoctoral Associate, PhD chemical and biomolecular engineering, Yonsei University)

- This research was presented at technical conferences and in publications to receive feedback and develop new ideas with the broader scientific community. The team disseminated this research in the following publications and presentations:
  - Emerson, HP, JE Szecsody, C Halter, J Robinson, CT Resch, and VL Freedman. (2024) "Spectral induced polarization of sulfur modified iron in sediments." *Journal of Contaminant Hydrology*. (Accepted September 2024).
  - J Thomle, L Slater, A Mangel, and HP Emerson. (2024) "An alternative electrode design for accurate spectral induced polarization measurements in variably saturated porous media." *Geophysical Journal International*. (Under Revision October 2024, submitted to Special Issue)
  - *Monitoring sulfur modified iron oxidation in sediments via spectral induced polarization,* HP Emerson, JE Szecsody, J Robinson, L Slater, 7th International IP Workshop, Lund, Sweden, May 28-30, 2024.
  - *Assessing the relationship between spectral induced polarization and geochemical alteration of zero valent iron during corrosion*, Z Vincent, JN Thomle, NP Qafoku, JE Szecsody, F Day-Lewis, C Zeng, and HP Emerson, Goldschmidt 2024, Chicago, IL, Aug. 18-24, 2024.
  - *Near Surface Petrophysics Panel*, International Meeting for Applied Geoscience and Energy (IMAGE) 2024, HP Emerson, Houston, TX, Aug. 26-29, 2024.

2.0 Critical Review of Laboratory-Scale SIP

A series of hybrid meetings were conducted with a team of subject matter experts to review data collected previously in FY20-FY22 and summarized in a previous report (Emerson et al. 2021). The critical review team consisted of experts in the following areas:

- Field-scale geophysics: Fred Day-Lewis, Chris Strickland, Jonathan Thomle
- Computational geophysics: Timothy C. Johnson, Judy Robinson
- Spectral induced polarization: Lee Slater, Klaudio Peshtani
- Geochemistry: Jim Szecsody, Nikolla Qafoku, Hilary Emerson
- Hanford Site remediation and hydrology: Rob Mackley, Inci Demirkanli
- Electrochemistry: Chao Zeng

Meetings were focused on reviewing the SIP responses of different remediation technologies within 1D column experiments. The SIP data for different groups of amendments were reviewed at separate meetings. The team focused on cross-disciplinary discussions to understand the geochemical reactions and physical changes in these systems following treatment with different amendments in addition to the observed polarization responses for these systems. Separate meetings covered (i) apatite forming solutions, (ii) reductants, and (iii) two-step amendment technologies.

2.1 Evaluation of Previous Experimental Testing

Although previous testing results are summarized in a report (Emerson et al. 2021), the critical review team further evaluated the experimental design and results. A preliminary analysis and data fitting via standard Cole-Cole models (Leroy et al. 2008) were achieved using the SIPy Studio software.

The team acknowledged that most of the data collected previously were of good quality and showed significant promise for monitoring amendment delivery and reactivity. Results for SMI and zero valent iron were summarized in a publication that was accepted to the *Journal of Contaminant Hydrology* in September 2024 and used for additional modeling (Section 3.2).

Several challenges were identified:

- SIP signals recorded in these experiments were clearly highly sensitive to geochemical conditions within the columns. However, moving toward a more quantitative interpretation of the results will require additional solid phase characterization following treatment of sediments with different amendments. For example, X-ray computed microtomography (XCT) could be used to identify changes in porosity induced by precipitation of amendments and X-ray magnetic circular dichroism (XMCD) could be used to identify magnetic mineral formation (e.g., magnetite). If we can identify the different physical and geochemical changes induced by an amendment, we can correlate these changes with the SIP response. These additional data are being collected for the Ca-Cit-PO_4 column experiments (XCT) and the previous SMI experiments (XMCD).
- A review of the data collected previously showed that most data are of high quality. However, select data sets were identified with inconsistencies due to potential electrode degradation and desaturation over time. The team redesigned the laboratory-scale columns and electrodes to enable better contact with porewater and repeatability of measurements over time in long-term experiments. Specific changes included (i) longer length and wider diameter columns, (ii) larger holes at electrode contacts

and more spacing between potential electrodes, and (iii) switching from wire point electrodes to porous disc electrodes for potential measurements to improve contact via increased surface area.

- Additional testing was initiated based on recommendations for some amendments (i.e., calcium citrate phosphate, Ca-Cit-PO_4, as discussed in Section 3.1). These experiments used the newly designed columns and electrodes. Preliminary results are consistent with most of the previously collected data, confirming the quality of previous results.

2.2 Mechanistic Conceptual SIP Model

An extensive literature review was performed to (i) facilitate multidisciplinary discussions and understanding within the critical review team and (ii) evaluate the current state of SIP knowledge regarding interpreting geochemical changes in porous media. Based on this, a conceptual model was developed to help convey potential changes in SIP response based on different alterations occurring in porous media, as shown in Figure 1. Changes were separated based on whether a significant volume fraction of electron-conducting minerals was present.

In the absence of electron-conducting minerals, real conductivity or σ' is related to (i) electrolytic conduction, i.e., electromigration of ions through the pore fluid filling interconnected pores, and (ii) surface conductivity associated with the tangential displacement of ions within the EDL forming at mineral grain surfaces (Vinegar and Waxman 1984). The σ' generally changes very little with respect to frequency. In contrast, imaginary conductivity or σ'' is associated with polarization effects or temporary, reversible charge storage of ions within the EDL that are frequency dependent (Revil 2012), and this is the primary parameter evaluated in the SIP response in the presence of non-electron-conducting minerals. Changes that influence the solution conductivity or mineral surfaces and EDL are likely to affect the magnitude of the SIP response while impacts to the pore throat or particle size distribution may change the frequency of the response (i.e., relaxation time constant or τ).

In the presence of electron-conducting minerals, a significant polarization enhancement is observed due to the large, induced dipole moment in the electron-conducting mineral and an associated redistribution of charge in the electrolyte surrounding the mineral. Generally, we expect the SIP response to be relatively larger when electron-conducting minerals are present with the magnitude of the signal primarily based on the volume and distribution of the mineral (Placencia-Gómez et al. 2015; Gurin et al. 2018). Previous research also has shown that τ is dependent on the particle size, solution conductivity, and mineralogy for electron-conducting minerals (Gurin et al. 2019; Hupfer et al. 2016; Abdulsamad et al. 2017).When the polarization is associated with electron conductors, phase (ϕ) is a diagnostic parameter as it is directly proportional to chargeability, m, and therefore is strongly controlled by the volume concentration of electron conductors and only weakly dependent on the fluid chemistry. In contrast, in the case of polarization of electron conductors, the σ'' is strongly impacted by pore fluid chemistry.

In both cases (electron conducting and non-electron or insulating conducting mineral polarization), SIP also has demonstrated sensitivity to mineral surface reactions (e.g., adsorption, precipitation, dissolution, and biofilm growth, as shown in Figure 1a).

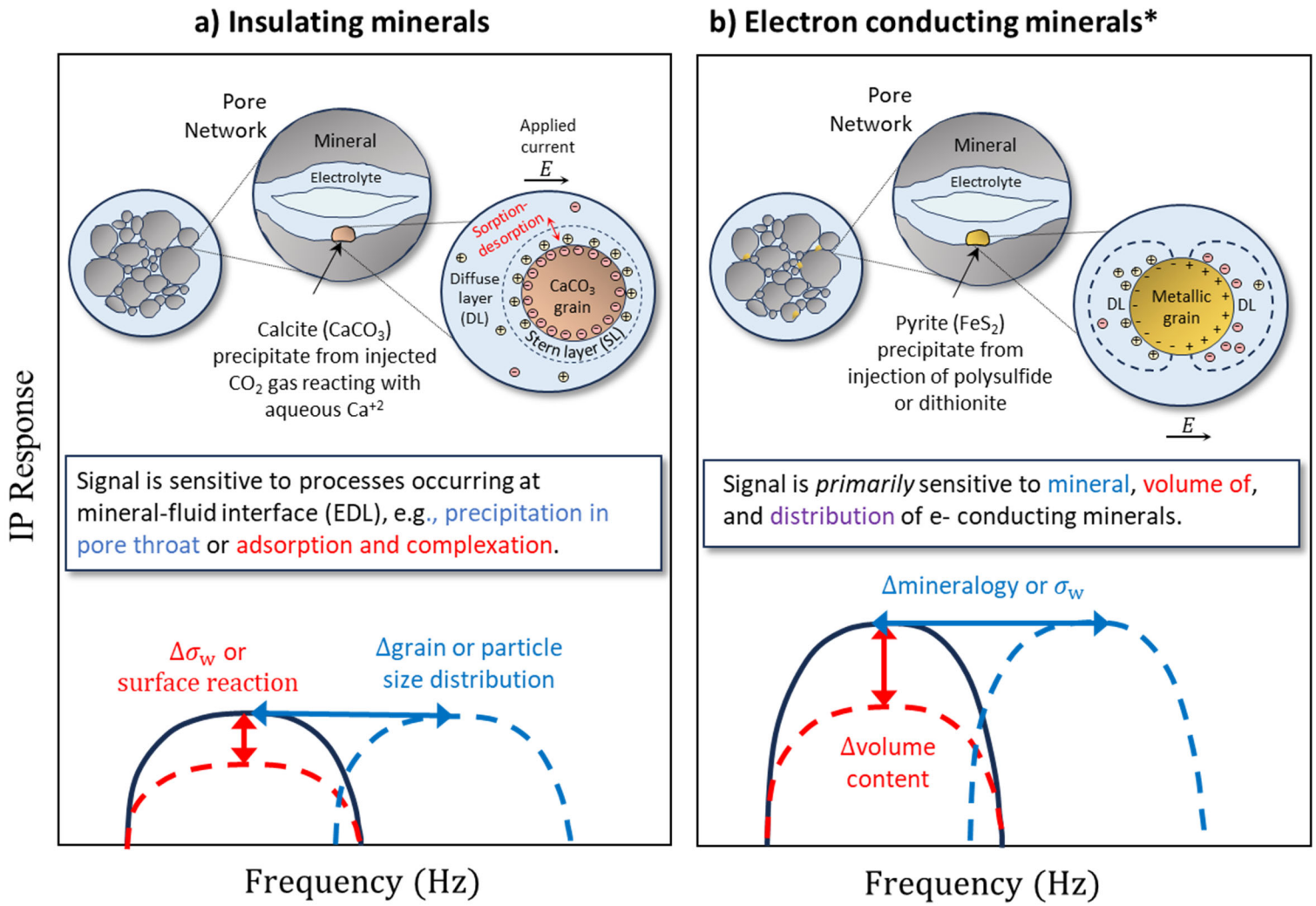

Figure 1. Conceptual model of the spectral induced polarization response as a change to a baseline (of background porous media) with insulating minerals (a) or electron conducting minerals (b) undergoing physical and geochemical changes. Note: Δ refers to change, σ_w is fluid conductivity, arrows delineate change from baseline peak (*black solid line*) prior to amendment delivery and/or geochemical reaction (*dashed line*).

3.0 Preliminary Results

This section presents preliminary results for two different systems tested at the laboratory-scale (Section 3.1) and simulations of laboratory-scale testing at field scale (Section 3.2) to demonstrate progress for two different remediation technologies: (i) a non-conductive amendment (apatite formed from calcium citrate phosphate, Ca-Cit-PO_4) and (ii) a conductive amendment (SMI). These data are preliminary, and all results should be considered as *for information only*. These data are in the process of being fully cleared through a rigorous quality assurance and quality control (QAQC) process (Section 5.0).

3.1 Calcium Citrate Phosphate: 1D Laboratory-Scale Columns

Additional experiments were conducted based on preliminary results reported previously (Emerson et al. 2021) following recommendations from the critical review team as described in Section 2.1. Ca-Cit-PO_4 slowly precipitates apatite after biodegradation of citrate. Citrate is added because it strongly complexes with Ca, keeping it soluble during delivery of the amendment to the subsurface. Once the citrate is degraded, Ca is available to precipitate with PO_4 and form apatite. The citrate biodegradation also results in mild reducing conditions, which may reduce Tc(VII) (as TcO_4^-) and U(VI) aqueous species, leading to formation of low-solubility solid phases (e.g., TcO_2 and UO_2). During subsequent apatite precipitation, reduced Tc and U phases may be adsorbed or coated by apatite, with remaining U(VI) also potentially being incorporated into apatite and/or forming autunite as depicted for Ca-Cit-PO_4 in Figure 2.

Chemical sequestration using these liquid-phase amendments has been demonstrated previously in the field along the River Corridor at the Hanford Site for both U and Sr-90 via Ca-Cit-PO_4 and for U via Poly-PO_4 (Szecsody et al. 2020; Vermeul et al. 2009; Vermeul et al. 2014; HPRC 2016, 2010, 2020; Szecsody et al. 2010). Ca-Cit-PO_4 was also shown to be effective at the laboratory scale for Sr-90 (Robinson et al. 2023). Moreover, other sites have also implemented similar technologies for U sequestration (Szecsody et al. 2016; Lammers et al. 2017; Fuller et al. 2003).

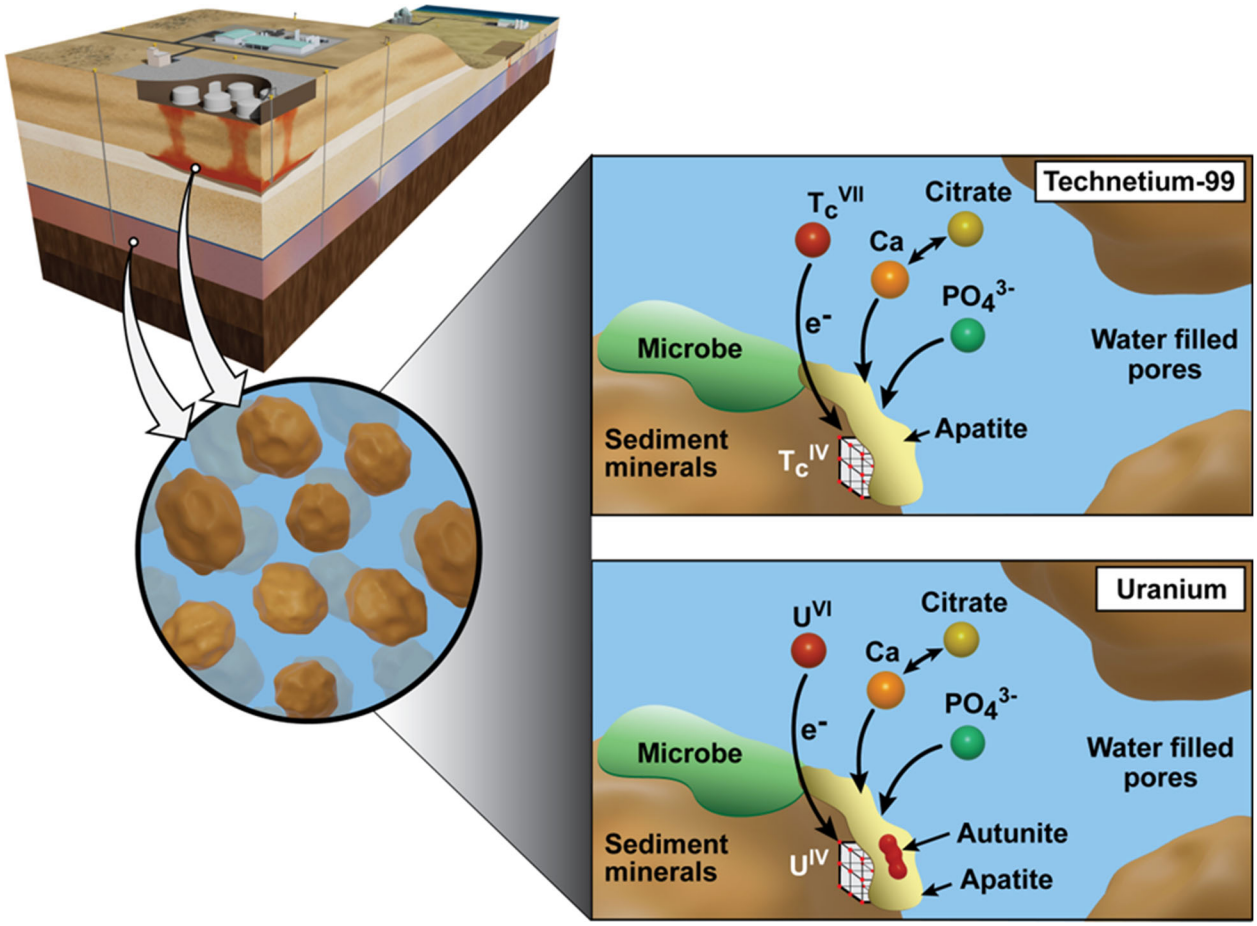

Figure 2. Sequestration of Tc (*top*) and U (*bottom*) in the saturated zone by treatment with a solution of Ca-Cit-PO_4 occurs simultaneously via the following processes: (*top*) citrate biodegradation to generate conditions for aqueous $Tc(VII)O_4^-$ and U(VI) reduction and precipitation as Tc(IV) and U(IV), (*bottom*) citrate degradation leaving Ca available to precipitate with PO_4 and form apatite, leading to coating of Tc(IV) and U(IV) by apatite as well as incorporation of U(VI) into autunite and apatite phases.

3.1.1 Results

Preliminary results for the treatment phase with the Ca-Cit-PO_4 amendment are summarized in

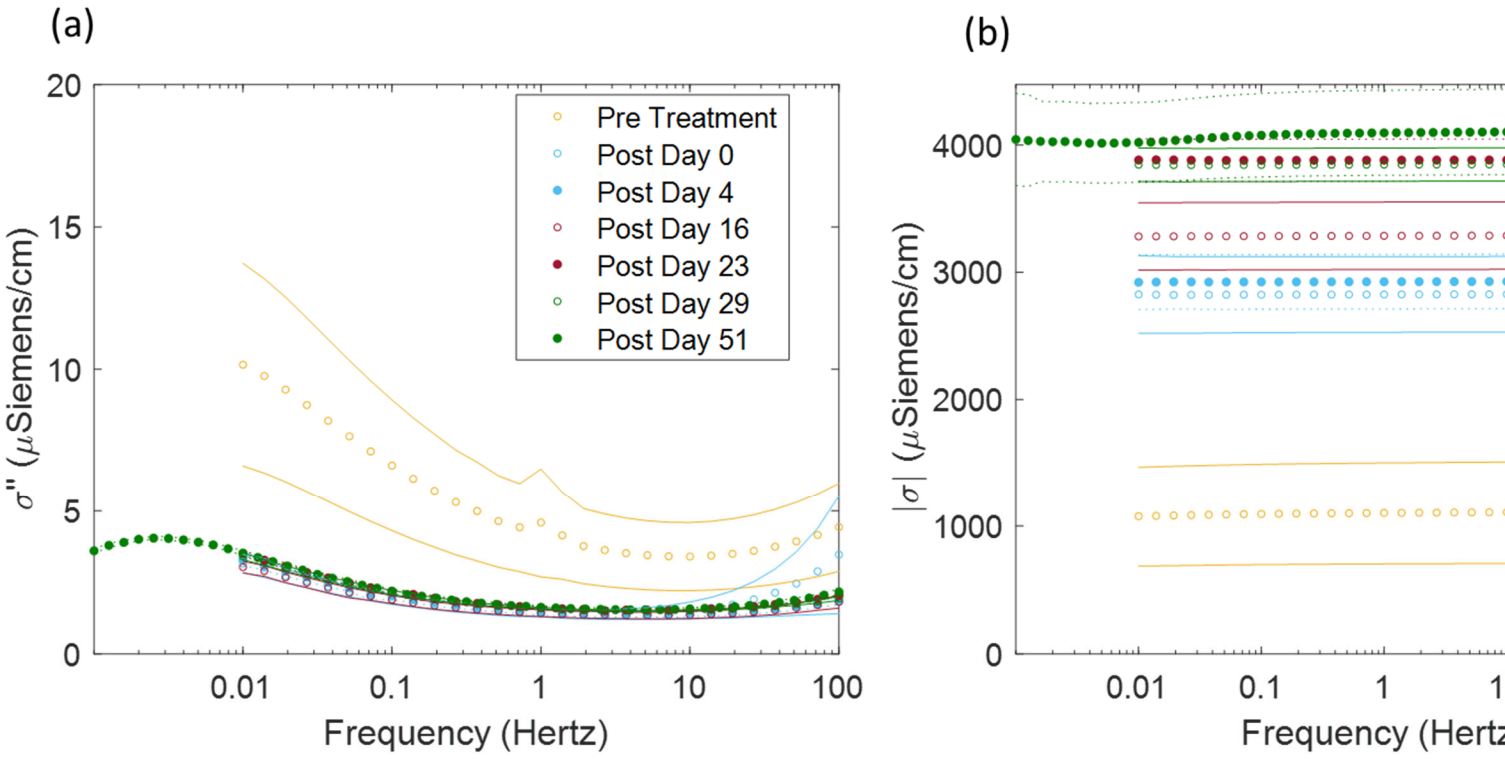

Figure 3. Following treatment, the σ' increases significantly due to the increased solution ionic strength while the σ'' (and ϕ) both decrease significantly following treatment. These data show that, in the absence of significant electron-conducting minerals, the increased solution conductivity from treatment with the amendment solution significantly impacts the magnitude of the SIP response. However, over time, there are other features observed in the σ'', including peaks between 1 and 10 Hz at around 23 days. These changes may indicate precipitation processes, although additional characterization is ongoing. In addition, XCT data will be collected prior to flushing of the columns to quantify potential changes in porosity due to amendment precipitation. Then, the columns will be flushed with synthetic groundwater to mimic a return to natural subsurface conditions (and lower solution conductivity) with additional monitoring over time.

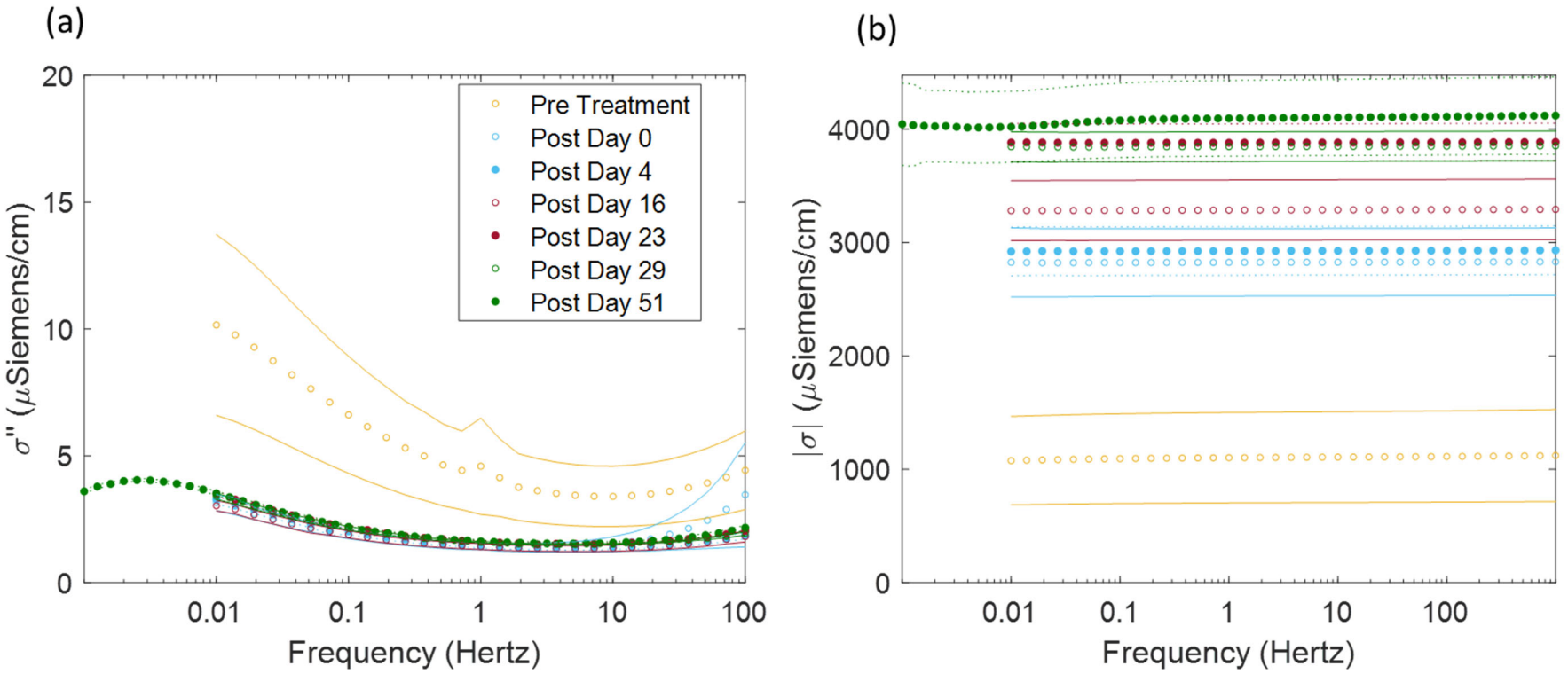

Figure 3. Five duplicate columns were treated with Ca-Cit-PO_4 and allowed to equilibrate over time for approximately 2 months, packed in Hanford sediments saturated with synthetic groundwater with (a) imaginary conductivity, σ″, in µS/cm and (b) real conductivity, σ', in µS/cm. Symbols represent the response for each frequency averaged across triplicate loops of data collected for five duplicate columns, with lines representing 95% confidence intervals for the columns. Note: At each time point where SIP data were collected, an aliquot of pore water was collected for characterization via injection of additional Ca-Cit-PO_4 to displace solution from the column.

3.2 Sulfur Modified Iron: Lab to Synthetic Field Simulation

SMI is a commonly used particulate amendment for subsurface remediation via reduction to lower solubility oxidation states (e.g., $Tc^{VII}O_4^-$ to TcO_2) or degradation (e.g., NO_3^- to N_2) as qualitatively represented in Figure 4. SMI is an electron-conducting mineral and therefore φ is strongly controlled by the volume concentration of electron conductors (Revil et al. 2015) and minimally influenced by fluid chemistry (unlike σ''). This material was used to demonstrate the potential for SIP in monitoring delivery and reactivity of electron-conducting amendments. Results from 1D column experiments were recently accepted for publication:

> Emerson, HP, JE Szecsody, C Halter, J Robinson, CT Resch, and VL Freedman. (2024) "Spectral induced polarization of sulfur modified iron in sediments." *Journal of Contaminant Hydrology*. (Accepted September 2024).

A summary of the SMI data is shown in Figure 5. A subset of these data was used for additional modeling efforts as described in the methods in Section 3.2.1, including the 2-day results for 10 wt% SMI. For the complete experimental methods and results from the column experiments, see the publication.

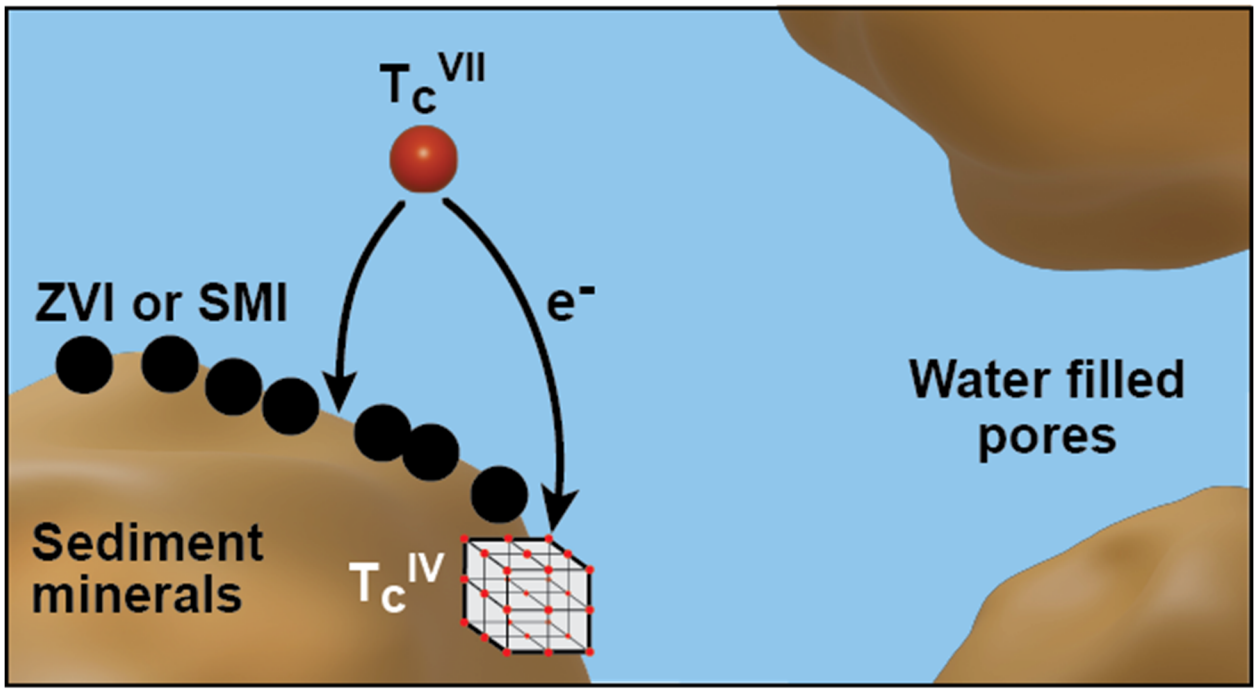

Figure 4. Example for reductive precipitation of Tc in the saturated zone by treatment with SMI to generate conditions for aqueous $Tc^{VII}O_4^-$ reduction and precipitation of Tc^{IV} as $Tc^{IV}O_2$ or $Tc^{IV}S_2$ type phases. During reaction of SMI with Tc, subsequent oxidation, dissolution, and precipitation of Fe from SMI occurs over time.

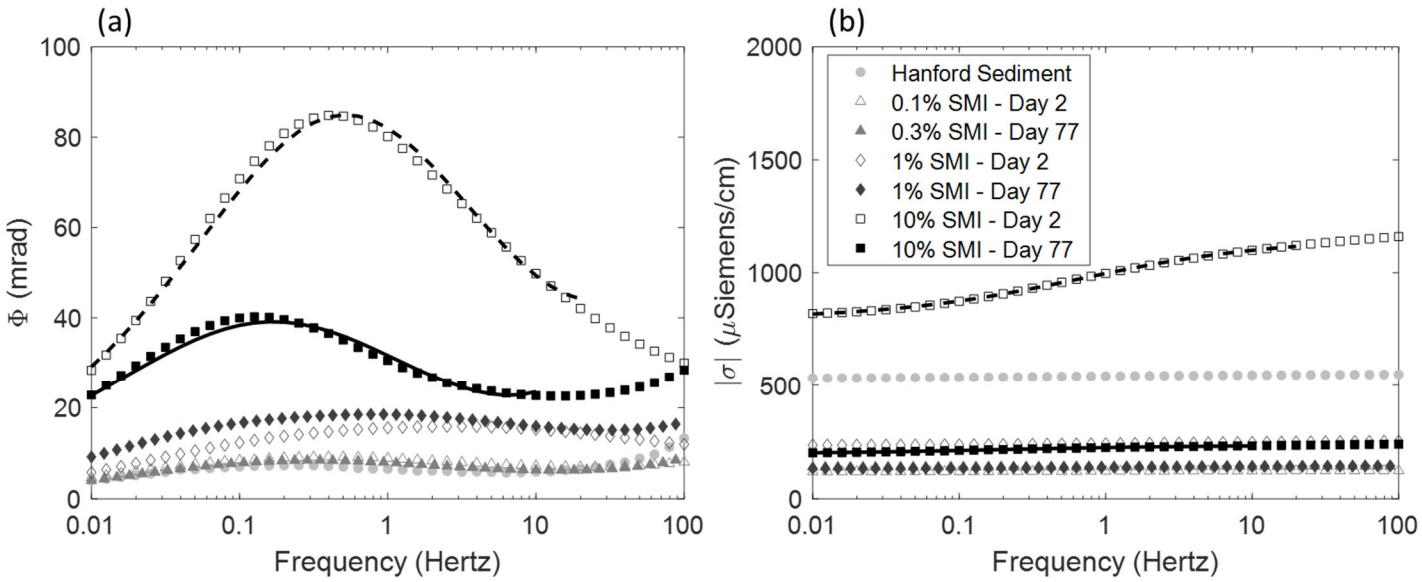

Figure 5. SMI at 0.1 to 10 wt% as monitored for change over time (aging) for up to 77 days, packed in Hanford sediments saturated with synthetic groundwater with (a) phase, ϕ, in mrad and (b) complex conductivity magnitude, |σ|, in μS/cm. Symbols represent the average response for each frequency with triplicate loops of data collected.

3.2.1 Methods

SMI SIP laboratory values of σ' and σ'' were used in synthetic E4D (Johnson 2014; Johnson et al. 2010) simulations to determine if the response observed in the laboratory could be imaged in the field. The synthetic field setup consisted of two blocks with dimensions of 2 m × 2 m × 2 m. One block was 1 m below the ground surface and the second block was 2.5 m below the ground surface (Figure 6). The blocks were chosen to be broadly representative of a field remedial application to a specified contaminated volume below the ground surface.

Synthetic SIP data were generated for the field simulations by using measured laboratory values. Baseline values for Hanford sediment were used within the homogeneous earth surrounding the two blocks (Figure 5). Within each block, the 10 wt% SMI values from day 2 were used (Figure 5). There was at least one order of magnitude difference in σ'' between these two datasets. SIP surface data was generated from 48 electrodes in a comprehensive survey of 2040 nested and dipole-dipole measurements. The electrode configuration consisted of 3 rows with 16 electrodes, spaced 1 m apart. Each row was separated by 5 m. The two blocks were centered below the middle row of electrodes (Figure 6). To generate the data, the two blocks were explicitly positioned within the finite element mesh. Table 1 lists the baseline and 10 wt% SIP data used within the homogeneous earth and blocks, respectively, to generate the synthetic SIP data.

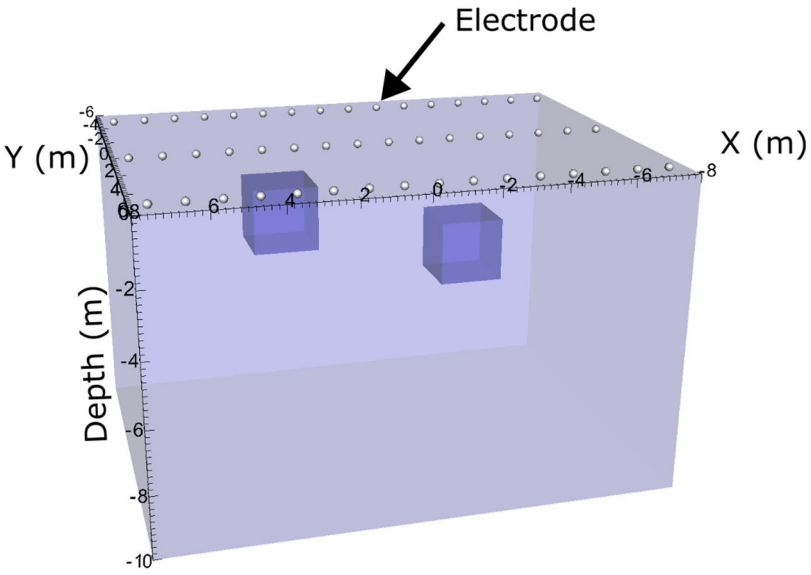

Figure 6. Two-block model used to broadly represent a field remedial application within a volume below the ground surface. The light purple region represents a homogeneous earth where SIP data on Hanford sediment (Figure 5) was used. The 10 wt% SMI laboratory data from day 2 were used within the boundaries of the two blocks (Figure 5).

The synthetically generated data was used as input to invert for a 3D SIP model. The finite element mesh for the inversion was homogeneous and did not contain the block regions shown in Figure 6. Smoothness constraints (e.g., nearest neighbor smoothing) were used between adjacent finite elements and the data were fit to assume 5% noise. SIP models consist of (i) σ', which is primarily representative of electrolytic conduction and also the output of an ERT inversion; and (ii) σ'' (refer to Section 2.2). The ϕ can be calculated as the ratio of σ''/σ'. The SIP images are representative of what could be expected if analogous laboratory conditions existed in the field with the electrode array shown.

For context, bulk conductivity from ERT has been used on the Hanford Site to monitor emplacement or spatial distribution of an injected amendment (Johnson et al. 2019b), including to indirectly determine where contaminants are located (Johnson et al. 2019a; Robinson et al. 2024). An ERT image can provide a 3D/4D (three-dimensional space plus time) vantage of where there is a change in electrical properties in the subsurface that coincide with a strong contrast or change in saturation, fluid conductivity, and/or porosity in the same location. While there may be small changes in bulk conductivity with frequency, it is generally not frequency dependent (Binley and Slater 2020).

Table 1. Baseline and 10 wt% SMI values (day 2) used in synthetic simulations for $\sigma'$and σ''. Baseline values were used within the surrounding volume and 10 wt% SMI values were used within each block (refer to Figure 6). Note there is at least an order of magnitude change between the baseline and 10 wt% SMI response in σ''.

	Baseline		10 wt% SMI	
Frequency (Hz)	σ'(S/m)	σ''(S/m)	σ'(S/m)	σ''(S/m)
100	3.24×10^{-3}	2.56×10^{-5}	3.32×10^{-2}	1.22×10^{-3}
10	3.22×10^{-3}	1.79×10^{-5}	3.11×10^{-2}	1.76×10^{-3}
1	3.19×10^{-3}	2.17×10^{-5}	2.79×10^{-2}	2.33×10^{-3}
0.1	3.15×10^{-3}	2.44×10^{-5}	2.44×10^{-2}	1.80×10^{-3}
0.01	3.12×10^{-3}	1.42×10^{-5}	2.28×10^{-2}	7.02×10^{-4}
0.001	3.20×10^{-3}	5.89×10^{-6}	2.72×10^{-2}	1.89×10^{-4}

3.2.2 Results

Figure 7 shows images across six orders of frequency as σ' and ϕ to summarize the most pertinent findings. First, the images show that the deeper block is not well resolved. An electrode array with larger electrode spacing or additional electrodes would be able to image deeper below the ground surface; this would require additional feasibility simulations to properly fine-tune the electrode spacing and measurement sequence. The shallow block is well resolved across the spectra, and therefore insights into the SIP interpretation (σ' and ϕ) will focus on this block.

The σ' in Figure 7 shows clearly where the SMI has been applied and there are small changes across the frequencies shown. This agrees with the laboratory data (Figure 5). The ϕ shows variability across the frequency spectra, which mimics the trend shown in the laboratory data. The ϕ indicates *where reactions are occurring* in contrast to σ', which shows *where the SMI has been emplaced*. The ϕ response of the reactions is frequency dependent; therefore, acquiring the full SIP spectra gives insight into (i) the full spatial extent of where reactions are occurring (e.g., collecting data at for example 100 Hz would show limited impact) and (ii) the overall polarizability, which can be related to the volume fraction of SMI (for concentrations < 10%) (Gurin et al. 2015).

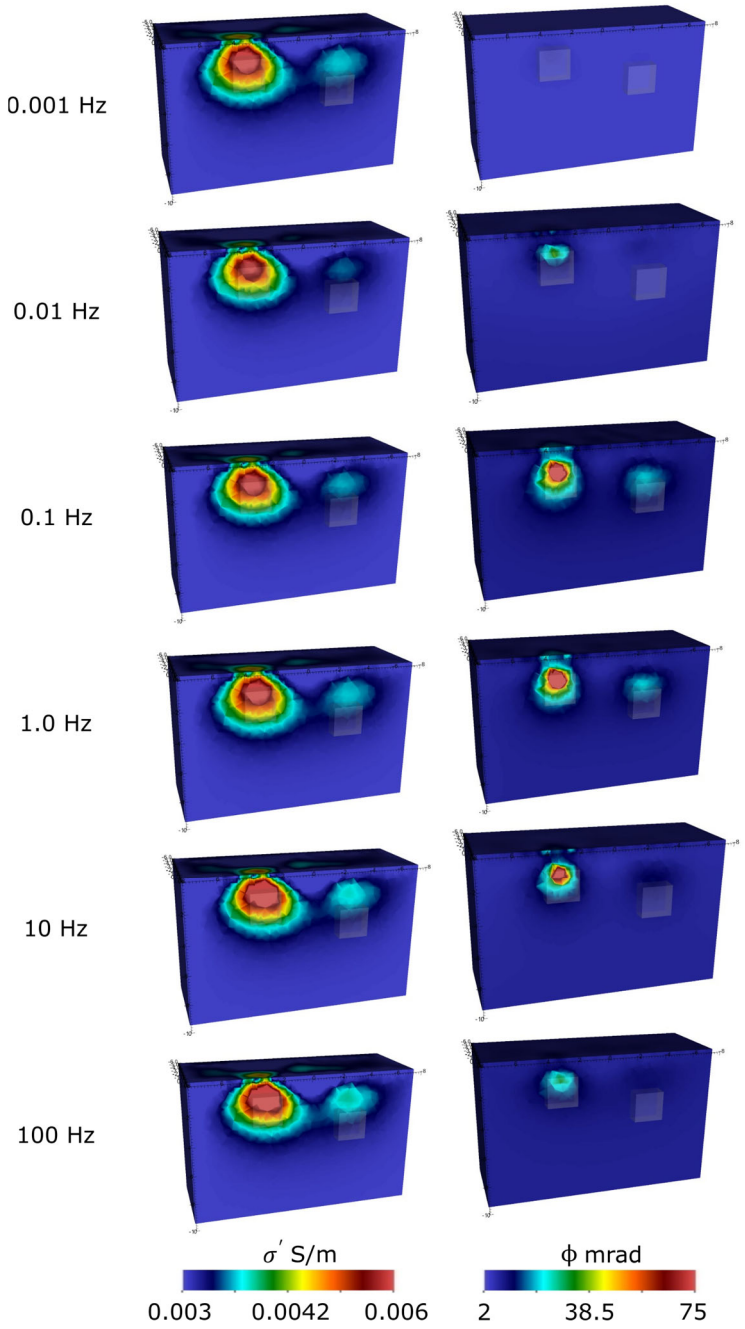

Figure 7. Inverted σ′ and ϕ for six frequencies demonstrating the spatial resolution of SIP imaging using laboratory-measured values. The shaded area represents the actual locations of the two blocks used in the modeling.

Figure 8 compares the ϕ for the true measured laboratory values used in the synthetic modeling to the resolved values in the shallow block. Similar to σ' values derived from ERT imaging, the ϕ images will be limited in resolution. This means that small-scale features may not be resolved, and larger features can appear smoothed or blurred compared to actual distributions (Johnson et al. 2019a). However, more generally, the trends and peak frequency are resolved, which are important considerations for field applicability.

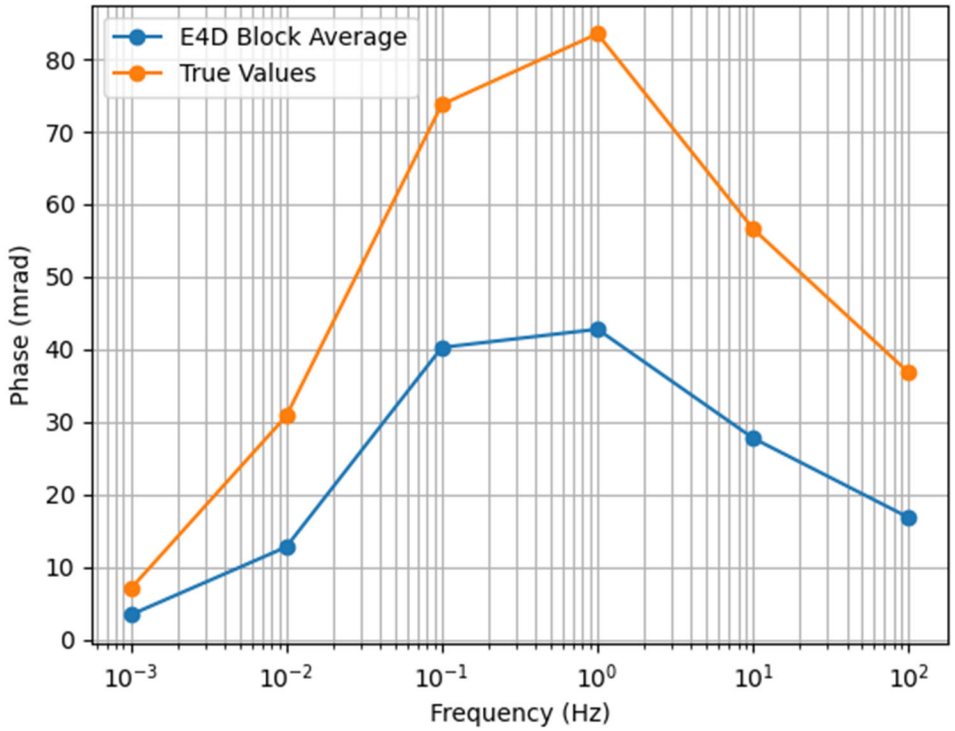

Figure 8. E4D-inverted averaged ϕ values shown with the actual/true laboratory measured values used in each block.

4.0 Proposed Framework for Evaluation

The critical review team outlined an approach for future work based on knowledge gaps identified for (i) our fundamental understanding of SIP and (ii) moving SIP from laboratory to field scale for monitoring of delivery and reactivity of amendments. Recommendations for experimental and modeling approaches are outlined in the following subsections; however, a test plan will be developed based on this proposed framework in FY25. Recommendations that are outside of the currently proposed 3-year scope of work under the Deep Vadose Zone program are marked with an asterisk (*). The interdisciplinary critical review team assembled for this work is uniquely positioned to help address these knowledge gaps with the team assembled including expertise in geochemistry, geophysics, and hydrogeology covering fundamental theory to field-scale systems.

4.1 Knowledge Gaps for Fundamental Understanding of SIP

There is a need to advance interpretation of SIP data by linking geochemical processes to the SIP response through more basic research. A fundamental understanding of these processes is paramount for interpreting the complex reactions occurring during remediation of the subsurface. The primary objective is to determine the specific geochemical reactions controlling changes to the SIP baseline (i.e., background porous media response) during delivery and reactivity of an amendment for sequestration or transformation of contaminants, including the shift in magnitude and frequency of the polarization response.

Milli- to micron-scale experimental and modeling efforts are recommended to improve our fundamental understanding of the processes controlling polarization of minerals and surfaces, including the following:

1. Measurement of SIP responses for different, simplified geochemical processes in highly controlled, well-characterized micro- to milli-fluidics experiments to better link geochemical processes to SIP responses.

   For example, previous researchers have predicted relatively small polarization responses for changes in grain size and roughness due to precipitation and sorption processes (Leroy et al. 2008; Vaudelet et al. 2011; Hao et al. 2015). However, the different processes are generally measured in separate experiments that are simplified and not comparable. The goal is to conduct experiments that can be used to interpret the SIP response in these more complex systems with real sediments and multiple geochemical reactions induced by delivery of a reactive amendment (e.g., emplacement of SMI with subsequent oxidation, precipitation, and dissolution of Fe).

2. Further development of approaches to model polarization mechanisms beyond Cole-Cole responses, including constraining models with physically meaningful properties.

   Results for real systems are often complex with multiple peaks or asymmetrical peaks in the SIP response that cannot be fit with Cole-Cole type models developed previously (Dias 2000; Gurin et al. 2015; Bücker et al. 2018; Bücker et al. 2019). However, these methods are generally empirical fits that are adjusted to match experimental observations. Therefore, we recommend further developing modeling approaches beginning with the Debye decomposition and/or Wong methods, which allows for greater flexibility in peak fitting and semi-empirical approaches, for application to real, complex systems (Nordsiek and Weller 2008; Wong 1979; Revil et al. 2014; Gurin et al. 2015).

3. *Combine reactive transport modeling with geophysical modeling to improve predictive power.

   The connection of SIP response to polarization mechanisms in the mineral and EDL to the geochemical reactions or processes would greatly improve our ability to predict the SIP response

from different geochemical reactions. However, significant theoretical development is needed. An example is the extension of parallel modeling developments with E4D and PFLOTRAN for prediction of electrical resistivity to include SIP (Jaysaval et al. 2023; Johnson et al. 2017) and proposed reactive transport extensions to recent developments in the Pore2Chip at the Environmental Molecular Sciences Laboratory (https://www.emsl.pnnl.gov/science/instruments-resources/terraforms-pore2chip).

4.2 Knowledge Gaps for Laboratory- to Field-Scale Testing

While our ability to use SIP in the field is dependent on the fundamental objectives outlined in Section 4.1, additional experimental and modeling recommendations are outlined in this section. The specific objectives include (i) quantifying the scalability of SIP response to the field, including the impact of heterogeneities, on our ability to detect changes in the SIP response; (ii) measuring the ability of SIP to monitor the changes induced by delivery of an amendment to the subsurface from a well (e.g., radial distribution of an amendment delivered from a well, changes in permeability, and porosity induced by amendments); and (iii) changes in reactivity of an amendment over time.

Column- to intermediate-scale experiments (cm to m) are recommended to demonstrate our ability to use SIP for field-scale monitoring, including the following:

1. Measurement of SIP response for additional amendments that are promising for the Hanford Site in 1D columns.

   The primary focus will be remediation technologies undergoing testing as part of the DV-1 treatability studies (DOE/RL 2019) and upcoming Ca-Cit-PO_4 injections in the 100 Area. Although preliminary data have been collected for many of these technologies, there are additional amendments that require testing. For example, tin apatite, calcium polysulfide, and bioremediation amendments have not yet been tested. Following the Phase 1 report for DV-1 treatability studies (Emerson et al. 2023), the most promising remaining technologies will be prioritized (e.g., tin apatite due to its significant promise for treatment of Tc-99).

2. Coordination for use of intermediate-scale testbeds for investigating the most promising amendments under saturated conditions.

   Parallel research is ongoing to develop an intermediate-scale system for the Geophysical Imaging of Flow and Transport (GIFT) system as described in a recent status report (Linneman et al. 2024). These systems are important to investigating more complex field-scale processes that we cannot measure in smaller column experiments, including spatial heterogeneity, flow pathways and scale-dependent diffusion/dispersion, and chemical gradients. This system is being constructed for intermediate-scale (meter-scale) monitoring and testing of remediation technologies.

   This is a valuable system for testing the SIP response for different remediation technologies and would be capable of testing the effects of (i) delivery of amendments radially from a well (i.e., chemical gradients), (ii) spatial heterogeneity in the subsurface, (iii) permeability reductions from precipitate formation following repeat injections of an amendment, and (iv) intermediate-scale hydrological effects (i.e., variable flow pathways and scale-dependent diffusion/dispersion). Most of the current research has focused on small, 1D columns in homogenous systems except for preliminary testing of reductants in 2D systems with simplified sand and iron lenses (Szecsody et al. 2023). Although these controlled experiments are vital for mechanistic interpretation of SIP datasets, we also need to understand the response in complex, heterogeneous systems to confirm feasibility for scaleup.

3. *Conduct unsaturated column and/or lysimeter testing to understand the impact of moisture content on our ability to measure the change in SIP response from delivery and reactivity of amendments.

   Research has shown that changes in porosity and water saturation significantly impact the polarization response of different consolidated (e.g., sandstone or mudstone) and unconsolidated (sand or gravel) materials (Peshtani et al. 2024; Revil et al. 2023; Binley et al. 2005). The SIP response has been effectively modeled in simplified systems with different subsurface materials with varying water saturation (e.g., clay and sandstone materials in Revil et al. 2023 and Binley et al. 2005, respectively). However, it is unclear how changes in water saturation may impact our ability to monitor geochemical reactions induced by amendments. This must be considered for potential technologies to be applied in vadose zone conditions.

Further field-scale modeling (meters to tens of meters) is recommended to understand the sensitivity of SIP as systems become larger and more heterogeneous, including the following:

1. Sensitivity modeling of detectability of amendments and reactions based on laboratory-scale experimental results.

   Preliminary modeling presented in Section 3.2 highlights the potential for monitoring amendment delivery and reactivity in the field. However, there is a need to extend this work to more complex systems and methods, including (i) subsurface heterogeneity, (ii) sensitivity across space (e.g., estimation of a transfer function or filter), (iii) comparing surface versus down-hole borehole arrays, (iv) different methods of calculating (e.g., depicting a baseline subtraction/ difference versus complex conductivity), and (v) different error estimation procedures (e.g., variable frequency errors).

2. Updates to computational tools to improve prediction abilities at field scale.

   For example, the current tools only allow for single frequency input and output and do not include variable frequency input and output (E4D; https://e4d-userguide.pnnl.gov/e4d_guide/e4d_citation.html).

5.0 Quality Assurance

This work was performed in accordance with the PNNL Nuclear Quality Assurance Program (NQAP). The NQAP complies with DOE Order 414.1D, *Quality Assurance*. The NQAP uses NQA-1-2012, *Quality Assurance Requirements for Nuclear Facility Application*, as its consensus standard and NQA-1-2012, Subpart 4.2.1 as the basis for its graded approach to quality. This work emphasized acquiring new theoretical or experimental knowledge. The information associated with this report should not be used as design input or operating parameters without additional qualification.

6.0 References

Abdulsamad, F., N. Florsch, and C. Camerlynck. 2017. "Spectral Induced Polarization in a Sandy Medium Containing Semiconductor Materials: Experimental Results and Numerical Modelling of the Polarization Mechanism." *Near Surface Geophysics* 15 (6): 669-683.

Binley, A., and L. Slater. 2020. *Resistivity and Induced Polarization: Theory and Applications to the near-Surface Earth*. Edited by Cambridge University Press.

Binley, A., L. D. Slater, M. Fukes, and G. Cassiani. 2005. "Relationship between Spectral Induced Polarization and Hydraulic Properties of Saturated and Unsaturated Sandstone." *Water Resources Research* 41 (12).

Brunauer, S., P. H. Emmett, and E. Teller. 1938. "Adsorption of Gases in Multimolecular Layers." *Journal of the American Chemical Society* 60 (2): 309-319.

Bücker, M., A. F. Orozco, and A. Kemna. 2018. "Electrochemical Polarization around Metallic Particles—Part 1: The Role of Diffuse-Layer and Volume-Diffusion Relaxation." *Geophysics* 83 (4): E203-E217.

Bücker, M., S. Undorf, A. Flores Orozco, and A. Kemna. 2019. "Electrochemical Polarization around Metallic Particles—Part 2: The Role of Diffuse Surface Charge." *Geophysics* 84 (2): E57-E73.

Dias, C. A. 2000. "Developments in a Model to Describe Low-Frequency Electrical Polarization of Rocks." *Geophysics* 65 (2): 437-451.

DOE/RL. 2019. *200-Dv-1 Operable Unit Laboratory Treatability Study Test Plan.* DOE/RL-2019-28 Rev 0.0. Department of Energy Richland Office Richland, WA.

Emerson, H. P., J. Szecsody, A. Lawter, C. Halter, A. Mangel, E. Fernald, C. T. Resch, K. Muller, C. E. Bagwell, M. E. Bowden, O. Qafoku, J. N. Thomle, N. P. Qafoku, and V. L. Freedman. 2021. *Spectral Induced Polarization-Biogeochemical Relationships for Remediation Amendment Monitoring.* PNNL-30440 Rev 1. Pacific Northwest National Laboratory Richland, WA.

Emerson, H. P., J. E. Szecsody, A. R. Lawter, K. Bagwell, M. M. V. Snyder, K. A. Muller, A. E. Plymale, D. L. Saunders, J. R. Hager, N. M. Escobedo, G. Wang, C. T. Resch, K. Bailey, J. Torgeson, C. I. Pearce, S. Hoyle, S. R. Baum, I. I. Leavy, K. Rue, L. Hibbard, M. Doughman, E. A. Cordova, D. I. Demirkanli, and N. Huerta. 2023. *200-Dv-1 Laboratory Treatability Testing Project: Proof-of-Principle Results.* PNNL-34300 Rev 0.0. Pacific Northwest National Laboratory Richland, WA.

Fuller, C., J. Bargar, and J. Davis. 2003. "Molecular-Scale Characterization of Uranium Sorption by Bone Apatite Materials for a Permeable Reactive Barrier Demonstration." *Environ Sci Technol* 37 (20): 4642-4649.

Gurin, G., Y. Ilyin, S. Nilov, D. Ivanov, E. Kozlov, and K. Titov. 2018. "Induced Polarization of Rocks Containing Pyrite: Interpretation Based on X-Ray Computed Tomography." *Journal of Applied Geophysics* 154: 50-63.

Gurin, G., A. Tarasov, Y. Il'in, and K. Titov. 2015. "Application of the Debye Decomposition Approach to Analysis of Induced-Polarization Profiling Data (Julietta Gold-Silver Deposit, Magadan Region)." *Russian Geology and Geophysics* 56: 1757-1771.

Gurin, G., K. Titov, and Y. Ilyin. 2019. "Induced Polarization of Rocks Containing Metallic Particles: Evidence of Passivation Effect." *Geophysical Research Letters* 46 (2): 670-677.

Hao, N., S. M. Moysey, B. A. Powell, and D. Ntarlagiannis. 2015. "Evaluation of Surface Sorption Processes Using Spectral Induced Polarization and a 22na Tracer." *Environ Sci Technol* 49 (16): 9866-9873.

HPRC, C. M. 2010. *Treatability Test Report for Field-Scale Apatite Jet Injection Demonstration for the 100-Nr-2 Operable Unit.* SGW-47062. CH2M Hill Plateau Remediation Company Richland, WA.

HPRC, C. M. 2016. *300-Ff5 Operable Unit Enhanced Attenuation Stage a Delivery Performance Report.* SGW-59614 Rev 0.0. CH2M Hill Plateau Remediation Company Richland, WA.

HPRC, C. M. 2020. *300-Ff-5 Operable Unit Enhanced Attenuation Uranium Sequestration Completion Report.* SGW-63113 Rev 0.0. CH2M Hill Plateau Remediation Company Richland, WA.

Hupfer, S., T. Martin, A. Weller, T. Günther, K. Kuhn, V. D. N. Ngninjio, and U. Noell. 2016. "Polarization Effects of Unconsolidated Sulphide-Sand-Mixtures." *Journal of Applied Geophysics* 135: 456-465.

Jaysaval, P., G. E. Hammond, and T. C. Johnson. 2023. "Massively Parallel Modeling and Inversion of Electrical Resistivity Tomography Data Using Pflotran." *Geoscientific Model Development* 16 (3): 961-976.

Johnson, T., J. Thomle, J. Robinson, and I. Demirkanli. 2019a. *Electrical Resistivity Tomography of the 216-U-5 and 216-U-6 Wa-1 Waste Sites.* PNNL-29430. Pacific Northwest National Laboratory. Richland, WA.

Johnson, T., J. Thomle, J. Robinson, R. Mackley, and M. Truex. 2019b. *Stage B Uranium Sequestration Amendment Delivery Monitoring Using Time-Lapse Electrical Resistivity Tomography.* PNNL-28619 Rev 0.0. Pacific Northwest National Laboratory Richland, WA.

Johnson, T. C. 2014. *E4d : A Distributed Memory Parallel Electrical Geophysical Modeling and Inversion Code User Guide - Version 1.0.* Pacific Northwest National Laboratory Richland, WA.

Johnson, T. C., G. E. Hammond, and X. Chen. 2017. "Pflotran-E4d: A Parallel Open Source Pflotran Module for Simulating Time-Lapse Electrical Resistivity Data." *Computers & Geosciences* 99: 72-80.

Johnson, T. C., R. J. Versteeg, A. Ward, F. D. Day-Lewis, and A. Revil. 2010. "Improved Hydrogeophysical Characterization and Monitoring through Parallel Modeling and Inversion of Time-Domain Resistivity and Induced-Polarization Data." *Geophysics* 75 (4).

Lammers, L. N., H. Rasmussen, D. Adilman, J. L. deLemos, P. Zeeb, D. G. Larson, and A. N. Quicksall. 2017. "Groundwater Uranium Stabilization by a Metastable Hydroxyapatite." *Applied Geochemistry* 84: 105-113.

Lawter, A., T. Levitskaia, O. Qafoku, M. Bowden, F. Colon, and N. Qafoku. 2021. "Simultaneous Immobilization of Aqueous Co-Contaminants Using a Bismuth Layered Material." *J Environ Radioact* 237: 106711.

Leroy, P., A. Revil, A. Kemna, P. Cosenza, and A. Ghorbani. 2008. "Complex Conductivity of Water-Saturated Packs of Glass Beads." *J Colloid Interface Sci* 321 (1): 103-117.

Linneman, D., C. E. Strickland, J. Knox, D. Sirota, and C. Linneman. 2024. *Geophysical Imaging of Flow and Transport (Gift): Fy24 Status Report.* Pacific Northwest National Laboratory, Richland, WA.

McKinley, J. P., J. M. Zachara, J. Wan, D. E. McCready, and S. M. Heald. 2007. "Geochemical Controls on Contaminant Uranium in Vadose Hanford Formation Sediments at the 200 Area and 300 Area, Hanford Site, Washington." *Vadose Zone Journal* 6 (4): 1004-1017.

Nordsiek, S., and A. Weller. 2008. "A New Approach to Fitting Induced-Polarization Spectra." *Geophysics* 73 (6): F235-F245.

Peshtani, K., A. Weller, and L. Slater. 2024. "Permeability and Induced Polarization of Mudstones." *Water Resources Research* 60 (8): e2024WR037455.

Placencia-Gómez, E., A. Parviainen, L. Slater, and J. Leveinen. 2015. "Spectral Induced Polarization (Sip) Response of Mine Tailings." *J Contam Hydrol* 173: 8-24.

Revil, A. 2012. "Spectral Induced Polarization of Shaly Sands: Influence of the Electrical Double Layer." *Water Resources Research* 48 (2).

Revil, A., N. Florsch, and C. Camerlynck. 2014. "Spectral Induced Polarization Porosimetry." *Geophysical Journal International* 198 (2): 1016-1033.

Revil, A., N. Florsch, and D. Mao. 2015. "Induced Polarization Response of Porous Media with Metallic Particles — Part 1: A Theory for Disseminated Semiconductors." *Geophysics* 80 (5): D525-D538.

Revil, A., A. Ghorbani, D. Jougnot, and B. Yven. 2023. "Induced Polarization of Clay-Rich Materials—Part 1: The Effect of Desiccation." *Geophysics* 88 (4): MR195-MR210.

Robinson, C., S. Shaw, J. R. Lloyd, J. Graham, and K. Morris. 2023. "Phosphate (Bio) Mineralization Remediation of 90sr-Contaminated Groundwaters." *ACS ES&T Water* 3 (10): 3223-3234.

Robinson, J., T. Johnson, J. Thomle, J. Cambeiro, K. Peta, P. Jaysaval, and R. Mackley. 2024. "Interpretation of Large-Scale, Long-Term Electrical Geophysical Monitoring Guided by a Process Simulation." *Vadose Zone Journal*.

Serne, R., A. Ward, W. Um, B. Bjornstad, D. Rucker, D. Lanigan, and M. Benecke. 2009. *Electrical Resistivity Correlation to Vadose Zone Sediment and Pore-Water Composition for the Bc Cribs and Trenches Area.* PNNL-17821 Rev 0.0. Pacific Northwest National Laboratory Richland, WA.

Serne, R. J., N. P. Qafoku, J. E. Szecsody, and M. J. Truex. 2020. *Sediment Mineralogy Data Review for the Hanford Central Plateau.* PNNL-30443 Rev 0.0. Pacific Northwest National Laboratory Richland, WA.

Szecsody, J. E., H. P. Emerson, R. D. Mackley, C. T. Resch, B. N. Gartman, C. I. Pearce, S. A. Saslow, O. Qafoku, K. A. Rod, and M. K. Nims. 2020. *Evaluation of the Change in Uranium Mobility in Sediments from the Hanford 300-Ff-5 Stage B Polyphosphate Field Injection.* PNNL-29650 Rev 0.0. Pacific Northwest National Laboratory, Richland, WA.

Szecsody, J. E., R. M. Moore, M. Rigali, V. R. Vermeul, and J. Luellen. 2016. *Use of a Ca-Citrate-Phosphate Solution to Form Hydroxyapatite for Uranium Stabilization of Old Rifle Sediments: Laboratory Proof of Principle Studies.* PNNL-25303 Rev 0.0. Pacific Northwest National Laboratory, Richland, WA.

Szecsody, J. E., P. G. Tratnyek, T. C. Johnson, J. L. Robinson, E. Placencia-Gómez, M. Bradley, J. N. Thomle, M. Truex, C. T. Resch, and B. Gartman. 2023. *Characterization of Enhanced Subsurface Abiotic Reactivity with Electrical Resistivity Tomography / Induced Polarization.* PNNL-34386 Rev 0.0. Pacific Northwest National Laboratory, Richland, WA.

Szecsody, J. E., M. J. Truex, M. J. Zhong, T. C. Johnson, N. P. Qafoku, M. D. Williams, W. J. Greenwood, E. L. Wallin, J. D. Bargar, and D. K. Faurie. 2012. "Geochemical and Geophysical Changes During Ammonia Gas Treatment of Vadose Zone Sediments for Uranium Remediation." *Vadose Zone Journal*: 1-13.

Szecsody, J. E., V. R. Vermeul, J. S. Fruchter, M. D. Williams, M. L. Rockhold, N. Qafoku, and J. L. Phillips. 2010. *Hanford 100-N Area in Situ Apatite and Phosphate Emplacement by Groundwater and Jet Injection: Geochemical and Physical Core Analysis.* PNNL-19524 Rev 0.0. Pacific Northwest National Laboratory, Richland, WA.

Tarasov, A., and K. Titov. 2013. "On the Use of the Cole–Cole Equations in Spectral Induced Polarization." *Geophysical Journal International* 195 (1): 352-356.

Vaudelet, P., A. Revil, M. Schmutz, M. Franceschi, and P. Bégassat. 2011. "Induced Polarization Signatures of Cations Exhibiting Differential Sorption Behaviors in Saturated Sands." *Water Resources Research* 47 (2).

Vermeul, V. R., B. N. Bjornstad, B. G. Fritz, J. S. Fruchter, R. D. Mackley, D. Mendoza, D. Newcomer, M. L. Rockhold, D. M. Wellman, and M. D. Williams. 2009. "300 Area Uranium Stabilization through Polyphosphate Injection: Final Report." PNNL-18529 Rev 0.0. Pacific Northwest National Laboratory, Richland, WA.

Vermeul, V. R., J. E. Szecsody, B. G. Fritz, M. D. Williams, R. C. Moore, and J. S. Fruchter. 2014. "An Injectable Apatite Permeable Reactive Barrier for in Situ 90sr Immobilization." *Groundwater Monitoring & Remediation* 34 (2): 28-41.

Vinegar, H., and M. Waxman. 1984. "Induced Polarization of Shaly Sands." *Geophysics* 49 (8): 1267-1287.

Wong, J. 1979. "An Electrochemical Model of the Induced-Polarization Phenomenon in Disseminated Sulfide Ores." *Geophysics* 44 (7): 1245-1265.

Xie, Y., C. J. Murray, G. V. Last, and R. D. Mackley. 2003. *Mineralogical and Bulk-Rock Geochemical Signatures of Ringold and Hanford Formation Sediments.* PNNL-14202 Rev 0.0. Pacific Northwest National Laboratory, Richland, WA.

Appendix A – Calcium Citrate Phosphate Methods

A.1 Sediments

An uncontaminated Hanford formation (Hf) sediment was procured from the Central Pre-Mix Concrete Company's gravel pit located in Pasco, WA. This sediment was used for experiments as it is representative of the Hf, which covers a significant portion of the vadose zone in the Central Plateau subsurface and represents similar mineralogy across the different formations within the saturated zones. As collected, the sediment had a moisture content of approximately 6.2% and a particle density of 2.83 ± 0.04 g/cm^3. These sediments were also analyzed by X-ray diffraction and sieve analysis as shown in Table A.1 and Table A.2, respectively. The Brunauer–Emmett–Teller (BET) method of surface area measurement was also used and measured approximately 11.4 ± 2.0 m^2/g. This distribution is consistent with previous characterization of Central Plateau sediments (Xie et al. 2003; Serne et al. 2020).

The cation exchange capacity (CEC) of each sediment was not measured; however, an estimate was used based on previous characterization of similar sediments. For the Hf, previous estimates of CEC ranged from 1 to 5 meq per 100 g of sediment (Serne et al. 2020), 5.3 meq/100 g for B-Complex sediments (McKinley et al. 2007), and 3 to 9 meq/100 g (averaging 6.5) for BC crib boreholes (Serne et al. 2009) with approximately 77% of the exchange sites being Ca (Szecsody et al. 2012). A conservative assumption of 2 meq per 100 g total CEC with 77% as Ca was used, resulting in an estimated 0.0077 mmol Ca/g of sediment, although there may be additional Ca available from dissolution of other minerals (e.g., calcite).

Table A.1. Wentworth particle size distribution based on dry sieve analysis.

Classification	Hf
Gravel (> 2 mm)	13%
Sand (2 mm to 63 µm)	85%
Silt/Clay (< 63 µm)	1%

Table A.2. X-ray diffraction of the < 2-mm size fraction of sediments.

Mineral Name	Hf
Quartz	36%
Feldspar	45%
Mica	5%
Amphibole	4%
Pyroxene	10%
Chlorite	0%

A.2 Solutions

Synthetic groundwater (SGW) was injected to represent baseline conditions similar to natural groundwater. The SGW was based on cation and anion averages of 54 well samples from the 200-UP and 200-ZP operable units from 2010 to 2018 (Lawter et al. 2021) (Table A.3).

Table A.3. Synthetic groundwater with pH adjustment to approximately 7.8 with ionic strength of approximately 7.1 mmol/L and solution conductivity of approximately 300 µS/cm prior to reaction with Hf sediments.

Constituent	Concentration (mmol/L)
$MgSO_4$	0.37
$MgCl_2$	0.25
$CaCl_2$	1.07
$KHCO_3$	0.12
$NaHCO_3$	1.59

Ca-Cit-PO_4 was added based on previous research (Szecsody et al. 2016) requiring 1.67× Ca as there is PO_4 and 2.5× more citrate than Ca. However, total Ca and citrate are decreased based on the expected ratio of solid to liquid in columns and approximately 2 meq of Ca/100 g in sediments (Section A.1). The Ca-Cit-PO_4 amendment was added as (i) 70 mM total PO_4 with the following ratio of species: 81% Na_2HPO_4, 14% NaH_2PO_4, and 5% $(NH_4)_2HPO_4$; (ii) 37 mM Ca as $CaCl_2$; and (iii) 90 mM sodium citrate ($NaC_6H_5O_7$) to reduce the likelihood that solutions would immediately precipitate. Citrate ($C_6H_5O_7^-$) is degraded by naturally occurring bacteria, leading to a slower precipitation process and potentially stimulating bacteria that can generate reducing conditions.

All chemicals were ACS reagent grade or better in purity.

A.3 1D Columns

Custom-built columns were fabricated from polyvinyl chloride with connections in end caps and side ports to accommodate electrodes for the collection of SIP measurements as shown in Figure A.1. Columns were 1-inch inner diameter and 6.9 inches in length with 1.5 inches in-between potential electrodes.

Electrodes were inserted into the end caps (current injection electrodes) and the two ports along the column body (potential sensing electrodes). Current electrodes were made from from coiled 1.6-mm-diameter Ag wire and inserted into the end caps. Potential electrodes consisted of a porous Ag-AgCl disc (6 mm × 1 mm sintered disk electrode, BMD-6, Biomed Products, Inc., Truckee, CA) housed within two plastic fittings with super absorbent sponge filling the electrode housing to keep electrical contact with solutions in columns (7271T33, McMaster-Carr, Elmhurst, IL).

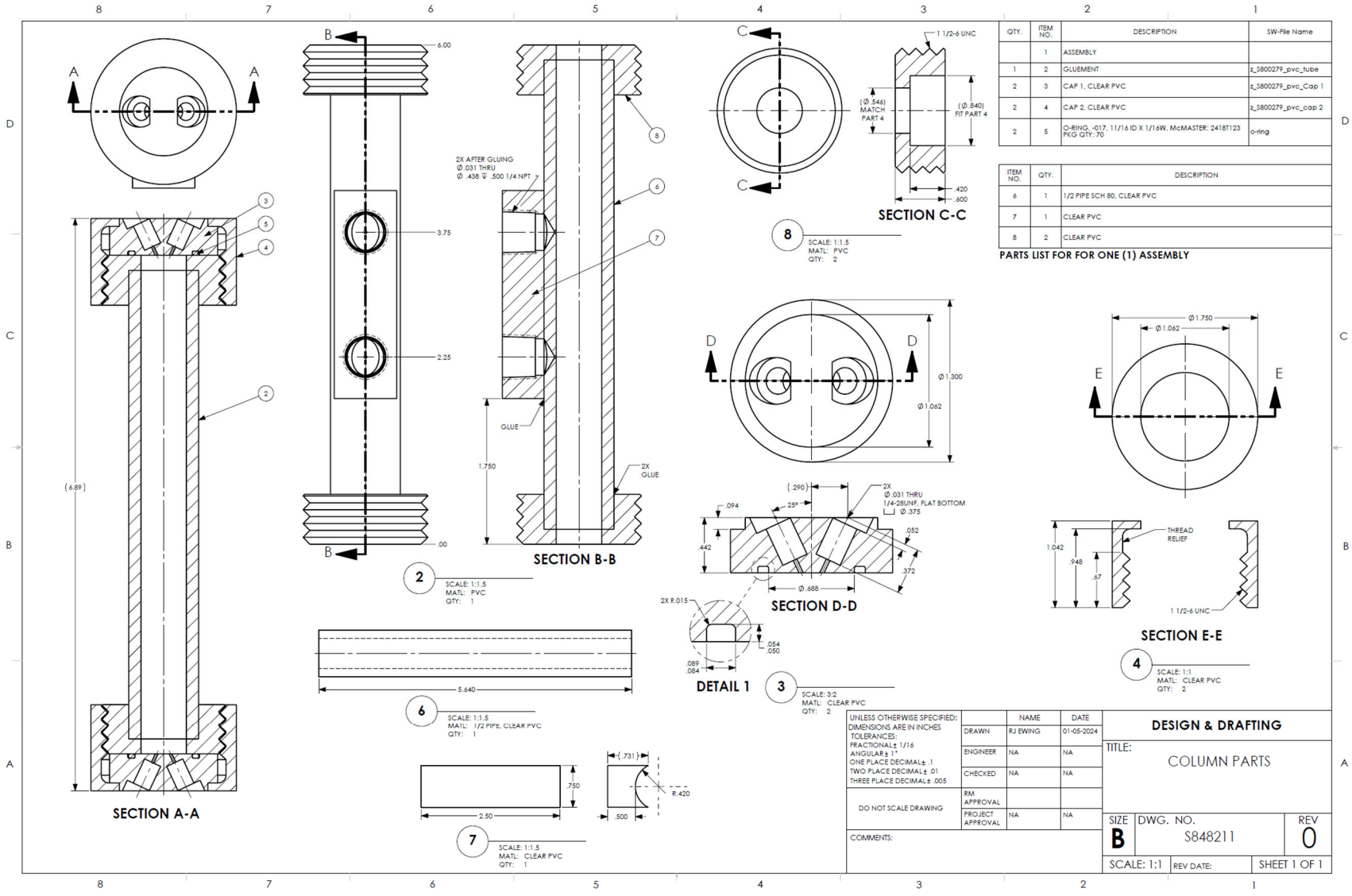

Figure A.1. AutoCAD schematic of the column design.

A.4 Methods

A.4.1 Column Experiments

Saturated column experiments were conducted with the columns described in Section A.3 with measurements collected over time, including SIP and additional secondary characterization at select time points throughout the different phases of experiments. The experimental matrix is presented in Table A.4 with approximate points for sacrificing columns. Experiments are ongoing and not all phases are complete.

- Phase 1: Collect baseline for all seven columns after saturating and equilibrating with SGW.
- Phase 2: Treat columns with Ca-Cit-PO_4 ("Treated-1 to Treated-5" columns only) and continue monitoring over time for approximately 10 weeks.
- Phase 3: Flush all columns with SGW and continue monitoring over time for at least 12 weeks.

At each time point for which SIP results are collected (detailed in the next section), effluent is also sampled for analysis and dissolved oxygen data are collected for influent and effluent end of column. In addition, X-ray computed microtomography data are collected for one time point following treatment and prior to sacrificing columns. Additional solid phase characterization was conducted on sediments prior to experiments and when columns were sacrificed. When columns were sacrificed, they were opened in an anaerobic chamber (N_2 atmosphere, Coy Laboratory Products, Grass Lake, MI). Sediments were homogenized in a beaker. Then, an aliquot was separated for air drying in the glovebox for X-ray diffraction (pXRD) and surface area (BET), while another aliquot of the moist sediments was subjected to acid extractions and measurement of moisture content.

Table A.4. Experimental matrix of column experiments

Experiment	Treatment	Sacrificial Sampling?
Control – 1	SGW	After Final Flush
Control – 2	SGW	After Final Flush
Treated - 1	Ca-Cit-PO_4	End of Treatment Phase
Treated – 2	Ca-Cit-PO_4	Immediately after Flush Phase
Treated – 3	Ca-Cit-PO_4	One Month after Flush Phase
Treated – 4	Ca-Cit-PO_4	After Final Flush
Treated – 5	Ca-Cit-PO_4	After Final Flush

A.4.2 Spectral Induced Polarization

All SIP measurements were collected using a portable SIP unit (Ontash & Ermac; River Edge, NJ). SIP measurements of sample impedance and ϕ were collected relative to a reference resistor from 0.01 to 10,000 Hz or 0.001 to 10,000 Hz, with collection of at least 30 measurements across the range of frequency. All SIP runs were collected in triplicate across the entire frequency range (i.e., three loops of data). The variability between runs was generally < 5%. SIP measurements were variable within the first few hours after saturation and treatment due to reactions occurring during equilibration of sediments with solution. Baseline SIP data were collected for sediments prior to treatment to confirm that SIP could effectively detect mineral alterations from an amendment as opposed to SIP changes from geochemical sediment heterogeneities.

The sample impedance (R, in Ω) was converted to complex resistivity based on the geometric factor (k, cm) as shown in Eq. (A.1). Then, the frequency-dependent complex conductivity (σ, in S/cm), the inverse of the complex resistivity (ρ, in Ω-cm), was calculated and represented by real (σ') and imaginary (σ'') components, or by a magnitude $|\sigma|$ and a phase ϕ, as shown in Eq. (A.2) (Binley and Slater 2020):

$$\sigma = \frac{1}{\rho} = \frac{1}{k \times R} \tag{A.1}$$

$$\sigma = \sigma' + i\sigma'' = |\sigma| e^{i\phi} \tag{A.2}$$

The ϕ represents the lag of the induced electric field behind the injected current, and, for ϕ < 100 mrad, it is approximately equal to the ratio σ''/σ'. The σ'' describes the reversible storage of charge (polarization), whereas the σ' describes the electromigration of charge (conduction). Therefore, ϕ represents the polarization strength relative to conduction strength.

The complex conductivity varies with frequency. The most popular way to represent this frequency dependence is through fitting a relaxation model. Here, data were fit to a Cole-Cole model shown in Eqs. (A.3) through (A.5) (Dias 2000; Tarasov and Titov 2013):

$$\sigma(\omega) = \sigma_\infty - \frac{\sigma_\infty - \sigma_0}{1 + (i\omega\tau)^c} = \sigma_0 \left[1 + \frac{m}{1-m}\left(1 - \frac{1}{1 + (i\omega\tau)^c(1-m)}\right)\right] \tag{A.3}$$

$$m = \frac{\sigma_\infty - \sigma_0}{\sigma_\infty} \tag{A.4}$$

$$f_p = \frac{1}{2\pi\tau} \tag{A.5}$$

In Eqs. (A.3) through (A.5), σ_0 and σ_∞ represent the low- and high-frequency values of σ, c is the Cole-Cole parameter that describes the steepness of the dispersion, τ is the relaxation time constant, m is intrinsic chargeability, f_p is the peak frequency in the imaginary conductivity, and ω is angular frequency ($\omega = 2\pi f$) (rad/sec^{-1}).

A.4.3 Secondary Characterization

A.4.3.1 Electrode Solution Methods

A specific conductance meter and electrode (Orion 013005MD electrode and Orion 4Star meter) were used to measure the conductivity for aqueous solutions injected into the columns with certified standards (Inorganic Ventures, 10 to 10,000 µS/cm) at each time point where SIP measurements were collected. Select samples were also analyzed for pH (Fisherbrand Accumet 13-620-183A electrode and Orion Star meter) and redox potential (Mettler Toledo Pt 4865-50-90-K9 electrode with Fisher Accumet XL150 meter).

A.4.3.2 Dissolved Oxygen

Dissolved oxygen was measured using PreSens oxygen spots (PSt3 sensor spots, Regensberg, Germany) installed approximately 0.5 inches inside the column from the inlet and outlet end caps. Measurements were collected simultaneously with each SIP measurement collected over time using their fiber optic cable and meter (OXY-1 SMA-BT meter) with data collected using the PreSens Wireless Studio software. At least 10 measurements were collected for each time point and averaged.

A.4.3.3 Inductively Coupled Plasma Optical Emission Spectroscopy

Select effluent and acid extraction solution samples were analyzed quantitatively for Al, Ba, Ca, Cr, Fe, Mg, Mn, Na, P, Si, and Sr using a PerkinElmer model Optima 2100DV with PerkinElmer S-93-plus auto-sampler. All samples and standards were diluted with 2% Fisher Scientific Optima trace metal grade nitric acid and twice deionized water with resistivity no less than 18.0 MΩ-cm. Samples were run at several dilutions to bring their elemental concentrations within the optimal analytical ranges of the instrument and to provide another level of result confirmation. An internal standard solution was added in-line to all samples, standards, and blanks to demonstrate the stability of the instrument and sample introduction system.

Minimum detection limits (MDLs) were established by running the lowest calibration standard seven consecutive times and multiplying the standard deviation of those seven replicates by 3.143 (student t-test value) to establish an instrument detection limit and then multiplying that number by 5 to get the MDL. This process was repeated three times on non-consecutive days and averaged to establish a working MDL in µg/L.

The instrument was calibrated using standards from the High-Purity Standards Corporation (Charleston, SC) or Inorganic Ventures, Inc. (Christiansburg, VA) to generate calibration curves. The range of the calibration curves for the PerkinElmer Optima 2100DV was 0.5 to 3000 µg/L. This calibration was verified with a verification standard immediately after calibration and during sample analysis every 10 samples, at a minimum. Calibration blanks were analyzed following each calibration verification to remove background signals, and potential carryover effects were not a factor. The calibration was independently verified using standards from Inorganic Ventures or High-Purity Standards, depending on which was used for the calibration as different sets of standards are used for calibration and verification.

A.4.3.4 Moisture Content

The mass of the moist sediment ($M_{wet\ sediment}$) in the column was determined by the difference in the empty column weight and packed column weight. Moisture content was measured on a separate aliquot of sediment by weighing 3 to 5 grams of moist sediment, drying for at least 48 hours at 105 °C, and weighing the dry sediment [$M_{dry\ sediment}$, Eqs. (A.6) to (A.7)]. Moisture content may be estimated on a dry or wet basis [Eq. (A.6), respectively]. The dry bulk density of the sediment was calculated from Eq. (A.8) based on these masses and the column volume (V). Next, the column was weighed again ($M_{sat,\ column}$) to calculate the pore volume (PV) and porosity (φ) as described in Eq. (A.9) and (A.10), respectively.

$$MC_{dry} = \frac{M_{wet\ sediment} - M_{dry\ sediment}}{M_{dry\ sediment}} \quad \text{(A.6)}$$

$$MC_{wet} = \frac{M_{wet\ sediment} - M_{dry\ sediment}}{M_{wet\ sediment}} \quad \text{(A.7)}$$

$$\rho_{bulk} = \frac{M_{dry\ sediment}}{V_{column}} = \frac{M_{wet\ sediment} \times (1 - MC_{wet})}{V_{column}} = \frac{M_{wet\ sediment}}{V_{column} \times (1 + MC_{dry})} \quad \text{(A.8)}$$

$$PV = M_{sat,column} - M_{dry\ sediment,column} \quad \text{(A.9)}$$

$$\varphi = \frac{M_{sat,column} - M_{dry\ sediment,column}}{V_{column}} \quad \text{(A.10)}$$

A.4.3.5 Acid Extractions

Acid extractions were conducted to confirm solid phase loading of Ca and P following treatment for sediments recovered from columns after sacrificing. 15 mL of 8 mol/L nitric acid is added to the tube containing approximately 5 grams of sediment and mixed intermittently for 2 to 3 hours at 95 °C or heated in a mod block without mixing (2 hours at 95 °C). After cooling, the tube is centrifuged at 3000 rpm for 10 minutes, then liquid is drawn off the top of the sediment and filtered with a syringe filter prior to analysis. 0.22-µm polytetrafluoroethylene filters were used to remove solids during sampling. A preparation blank was also prepared to check background contaminant concentrations and confirm that contaminants were soluble in extractions and results were reproducible.

A.4.3.6 Brunauer–Emmett–Teller Specific Surface Area

The surface area of solid samples in triplicates was obtained based on nitrogen adsorption isotherms using BET method (Brunauer et al. 1938) for Hf sediments prior to experiments and after sacrificial sampling of columns. The measurements were collected using Micromeritics, ASAP 2020 apparatus, after outgassing samples under vacuum at 75 °C for 640 minutes.

A.4.3.7 X-ray Diffraction Analysis

X-ray diffraction patterns (pXRD) were collected from powders crushed in a mortar and pestle and packed into zero-background well holders using a Rigaku SmartLab SE diffractometer for Hf sediment prior to experiments and after sacrificial sampling of columns. The instrument employed Bragg-Brentano geometry with a Cu X-ray source (λ = 1.5418 Å), a variable divergence slit, and a high-speed D/teX Ultra 250 1D detector. Patterns were collected between 2 and 100 °2θ at intervals of 0.01 °2θ and minerals identified through comparison with reference patterns in the ICDD database (International Center for Diffraction Data, PA).

Estimates of mineral concentrations were obtained by Rietveld fitting using Topas (v6, Bruker AXS). This method calculates the full diffraction profile from published crystal structures, applying convolutions for instrumental and specimen broadening arising from finite crystallite size and/or microstrain. Atomic coordinates were not refined, and instrumental parameters were also fixed after having been established from standard powders. For natural samples, the primary source of uncertainty for these determinations is the degree to which the published crystal structure of complex minerals matches that of the specimen. The fitting used fundamental parameter peak shapes and a spherical harmonics preferred orientation correction for the quartz peak intensities.

Pacific Northwest National Laboratory

902 Battelle Boulevard
P.O. Box 999
Richland, WA 99354
1-888-375-PNNL (7665)

www.pnnl.gov